

# Planar lightwave circuit devices for optical communication: present and future

Hiroshi Takahashi

NTT Photonics Laboratories, Nippon Telegraph and Telephone Corporation  
3-1 Morinosato Wakamiya, Atsugi, Kanagawa, 243-0198 Japan

## ABSTRACT

Silica-based planar lightwave circuits (PLC) are key components of functional devices designed for use in optical fiber communication systems because, compared with bulk optics devices, they offer compactness, excellent stability and reliability in addition to high functionality. This talk reviews the current status of PLC development. The fabrication process, basic characteristics, packaging and reliability are presented, many device applications are described, and experimental results related to optical switches, interleave filters, chromatic/polarization dispersion compensators, gain spectrum equalizers and wavelength multiplexers are reported. Finally, the history of PLC development is summarized, and future target devices are described along with the kind of development needed for such devices designed for use in the next generation of optical communication systems.

Keywords: Planar lightwave circuit, silica-based waveguide, arrayed-waveguide grating, Mach-Zehnder interferometer, WDM, wavelength multiplexer, optical switch, dispersion compensator, spectrum equalizer

## 1. INTRODUCTION

The huge demand for data communication resulting from the spread of the Internet will require DWDM systems with more wavelength channels and a higher transmission speed. This will necessitate a number of technical advances such as the improvement of wavelength multiplexers, and the realization of chromatic/polarization dispersion compensators, gain spectrum equalizers and certain new devices for use in novel modulation schemes. An additional research target involves the construction of photonic networks, where plural point-to-point DWDM transmission systems are connected and optical signals are treated as is (namely without OE/EO conversion at the nodes). Such systems require DWDM-based optical add/drop multiplexing (OADM) and optical cross connect (OXC) architectures, and large-scale integrated switches are key components.

Planar lightwave circuits (PLC) are key components of functional devices for use in such optical communication systems since, compared with bulk optics devices, they offer compactness and excellent stability in addition to intrinsic high functionality [1]. When a PLC device is composed of a silica glass waveguide, its insertion loss is very low because there is little absorption and scattering in the waveguide, and it provides high fiber coupling efficiency. In addition, PLC devices have long-term reliability thanks to the excellent physical and chemical stability of silica glass. These benefits are substantiated by the widespread use of arrayed-waveguide grating (AWG) wavelength multiplexers in practical DWDM systems and optical splitters in the subscriber lines of fiber-to-the-home systems.

Against this backdrop, we have been developing a number of silica-based PLC devices including splitters, switches, variable attenuators, interleave filters, wavelength multiplexers, dispersion compensators and spectrum equalizers to demonstrate the feasibility of PLC technology. This presentation describes the fabrication and basic characteristics of silica waveguides and reviews the device applications mentioned above introducing experimental results. Finally, the history of the development is summarized, and the next target devices are described along with the type of development required for such devices for use in the next generation of optical communication systems.

## 2. BASIC PLC TECHNOLOGY

### 2.1 SILICA-BASED OPTICAL WAVEGUIDE

Although it is generally possible to construct planar lightwave circuits with several kinds of material including dielectric crystals, semiconductors and polymers, for the following reasons we use silica-based glass waveguides. These waveguides have:

- 1) a low propagation loss
- 2) the same refractive index and mode field diameter as conventional single-mode fiber (low coupling loss and reflection)
- 3) excellent physical and chemical stability (they can withstand endface polishing for fiber coupling and have high long-term reliability)
- 4) they can be fabricated on an inexpensive large size Si wafer (low cost and large-scale) and
- 5) they offer easy phase controllability with a thin film heater via the thermo-optic effect.

Figure 1 shows the fabrication process and a cross-section of the silica waveguides we have developed [2]. We use flame hydrolysis deposition (FHD) for the silica glass layer deposition because of its high deposition rate since the cladding layer thickness should be 30  $\mu\text{m}$  or more. A white layer of fine particles (called silica soot) deposited by FHD becomes transparent glass film after high temperature treatment. The same procedure is repeated with  $\text{GeO}_2$ -doped silica glass for the core layer. Then the waveguide pattern is formed after photolithography and reactive ion etching. Finally, the upper cladding layer is deposited, again by FHD, to surround the core, as shown in the inset. The waveguide characteristics are summarized in Table 1. A lower refractive index difference ( $\Delta$ ) has lower propagation and fiber coupling losses and is suitable for simple devices such as Y-branch 1 x 8 splitters and wavelength-independent couplers. A higher  $\Delta$  waveguide has a small bending radius and is suitable for highly functional devices with complex waveguide layouts such as AWG wavelength multiplexers, thermo-optic switches and dispersion compensators.

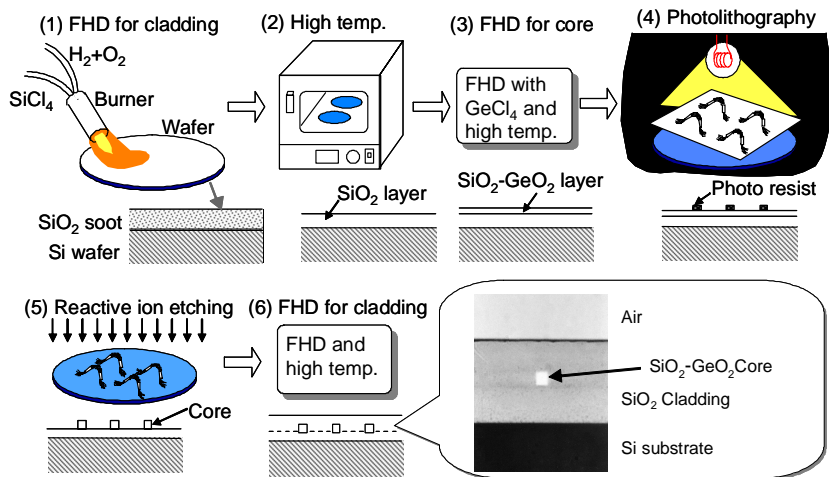


Fig. 1 Fabrication process and cross-section of silica-based waveguide

Table 1 Characteristics of silica-based waveguides

	Index difference	Core size	Bending radius	Propagation loss	SMF coupling loss	Typical applications
Low $\Delta$	0.25%	8 $\mu\text{m}$	25 mm	<0.01 dB/cm	<0.1 dB	Splitter, coupler
Medium $\Delta$	0.45%	7 $\mu\text{m}$	12 mm	0.02 dB/cm	0.1 dB	Large-scale splitter, coupler
High $\Delta$	0.75%	6 $\mu\text{m}$	5 mm	0.03 dB/cm	0.5 dB	AWG, switch, equalizer
Super high $\Delta$	1.5%	4.5 $\mu\text{m}$	2 mm	0.05 dB/cm	1.5 dB	Large-scale AWG, combination

## 2.2 PACKAGING AND RELIABILITY

In addition to the waveguide chip itself, packaging is an important issue as regards the practical use of PLC devices. This includes fiber attachment, electrical wiring for the thin film heater used as a phase shifter and the integration of a heater driver IC. We have developed all these items taking reliability into consideration.

**Fiber attachment:** Optical fibers are butt-coupled to the waveguide core. The fibers are aligned in a V-groove array on a glass block so that a large number can be attached simultaneously to the waveguide chip with excellent positional accuracy. The endface of the waveguide chip and fiber array are polished at an angle of 8 degrees to prevent reflection, and are fixed in place with UV curable adhesive. The adhesive was carefully developed in order to obtain sufficient adhesive strength, long-term reliability and resistance to high power incident light all at the same time. The maximum number of bundled fibers is currently 128.

**Fiber coupling loss reduction:** In general, the coupling loss caused by the spot size difference between a fiber and a silica waveguide is very low but it becomes obvious as the waveguide  $\Delta$  becomes higher. This loss can be reduced by introducing a tapered waveguide structure and an intermediate- $\Delta$  PLC between the fiber and waveguide as shown in Fig. 2 [3]. A super high (SH)  $\Delta$  waveguide with a 4.5  $\mu\text{m}$  square cross-section is widened through a tapered region to 6  $\mu\text{m}$  at the PLC chip end. The waveguide in the high (H)  $\Delta$  PLC is 6  $\mu\text{m}$  square on the SH $\Delta$  side and 9  $\mu\text{m}$  wide on the fiber side. With this structure, the coupling loss between a SH  $\Delta$  waveguide and single-mode fiber is reduced from 1.5 to 0.7 dB.

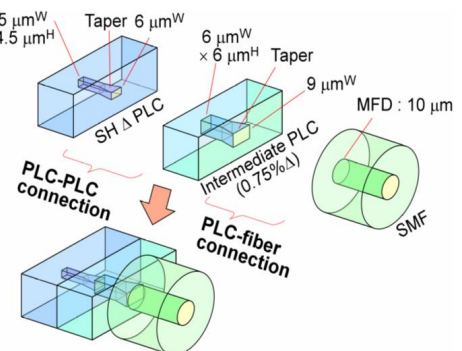


Fig. 2 Low loss coupling of SMF and SH  $\Delta$  WG

**Module structure:** Devices with basic functions such as splitters and couplers that do not need temperature control are very simple as shown in Fig. 3(a) where the PLC chip is pigtailed and packed in a plastic case. As regards temperature sensitive devices including AWG wavelength multiplexers, the PLC chip is mounted on a temperature stabilized plate and packaged in an adiabatic case as shown in Fig. 3(b). A thermo-electric cooler or an ohmic heater is used for temperature control. Figure 4 shows different types of packaging for PLC chips with thin film heaters for thermo-optic phase control. The conventional packaging (a) includes a printed wiring board (PWB) and a PLC chip. Each heater is connected to an electrical interface (pin/connector) through Au-wire bonding. The driver circuit is outside the module. Packaging (b) includes a heater driver IC on a PWB [4]. The merit of this type is that the driver IC controls the heater power and the user sends only the signal that indicates which heater should be activated. With packaging (c), bare driver IC chips are mounted directly on the PLC chip [5]. This design makes it possible to reduce the PLC chip size in addition to the PWB size because of the great reduction in the number of Au-wire bonding pads and the area needed for heater-to-pad wiring lines on the PLC chip surface. This effect becomes clear with a large scale PLC chip that includes a large number of heaters; for example, a 1 x 128 selection switch. In fact, the conventional 1 x 128 selection switch chip size is not determined by the lightwave circuit area but by the wiring area.



Fig. 3(a) PLC splitter



Fig. 3(b) AWG multi/demultiplexer

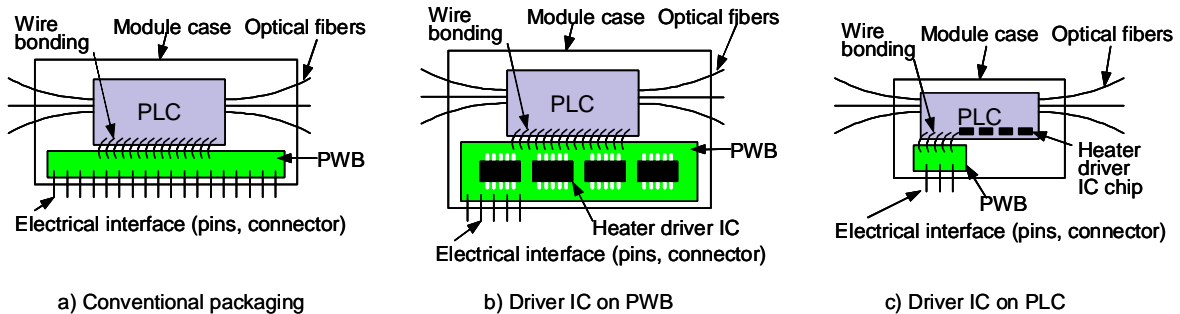


Fig. 4 Packaging types for PLC with thermo-optic phase shifter

**Reliability:** Many PLC modules like those shown in Fig. 3 were examined for many years under reliability test conditions based on Telcordia GR-1221-CORE and no problem was found [6]. The results confirm the reliability of the PLC chip and the fiber attachment and packaging design including the PLC chip mounting method. For this reason AWG multiplexers were introduced into practical WDM systems. Recently, we have also checked the reliability of heaters, wiring, Au-wire bonding, and bare driver IC mounting with the test modules shown in Fig 4(a, b and c) under the same conditions. In addition, accelerated tests on the heaters were undertaken with an electrical power greater than that usually employed. The modules passed all the tests.

### 3. MACH-ZEHNDER BASED OPTICAL SWITCHES

#### 3.1 MZI STRUCTURE AND CHARACTERISTICS

The Mach-Zehnder interferometer (MZI) structure shown in Fig. 5 is used for a 2 x 2 optical switch element [7]. The thin film heater on one of the two waveguides between the directional couplers works as a phase shifter based on the thermo-optic effect. When the heater is not activated, the MZI is in the *cross* state (#1 to #4, #2 to #3). When the heater is activated and the induced phase shift is  $\pi$ , the MZI is in the *through* state (#1 to #3, #2 to #4). The electrical power needed for a  $\pi$  phase shift is conventionally about 400 mW as shown in Fig. 6(a). A heat-insulating groove as shown in Fig. 6(b), which is formed by dry-etching the silica layer, can be used to reduce power consumption. The lowest power consumption yet obtained is 45 mW.

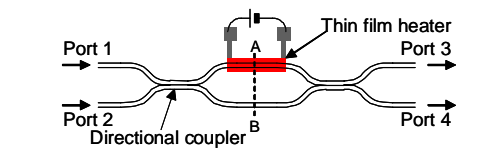


Fig.5 Waveguide layout of MZI

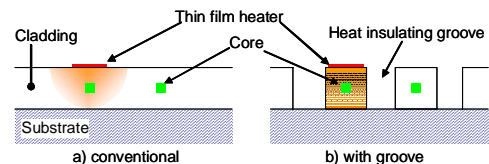


Fig.6 Cross section along A-B in Fig.5

The transmittance,  $T$ , of the MZI is described by the following equations:

$T = 1 - 2K(1-K)(1 + \cos\theta)$  for *through* paths (#1 to # 3 and #2 to #4)

$T = 2K(1-K)(1 + \cos\theta)$  for *cross* paths (#1 to # 4 and #2 to #3)

where  $K$  is the power coupling ratio of the directional couplers and  $\theta$  is the phase shift. Fabrication errors mean that  $K$  is not always 50%. This causes a degradation in the extinction ratio of the through path, namely  $T$  is not zero although  $\theta$  is set at 0. Meanwhile, for the cross path,  $T$  is always 0 at  $\theta = \pi$  whatever the value of  $K$  and we can always obtain a high extinction ratio even if there are fabrication induced variations in coupling ratio  $K$ . Figure 7 shows that the extinction ratio is independent of the ambient/chip temperature. This is because the transmittance is determined by not the absolute temperature, but by the temperature difference between the two waveguides. So none of the fabricated MZI-based switches described below are equipped with a temperature control system.

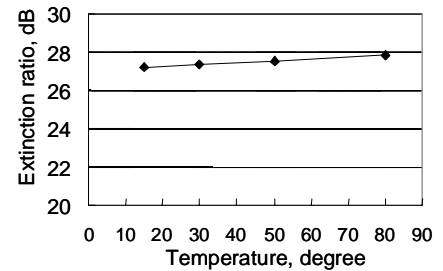


Fig.7 Ambient temperature vs extinction ratio of MZI switch cross path

The response time of the MZI is about 2 ms as shown in Fig. 8, which is the time it takes for the waveguide core to warm up. The response time can be improved by the technique described in the next section. Since the output optical power is uniquely determined by the applied electrical power, there is no ripple in the response and the repeatability of the output optical power is extremely high. This is one of the advantages of this switch, compared with conventional mechanical and MEMS switches.

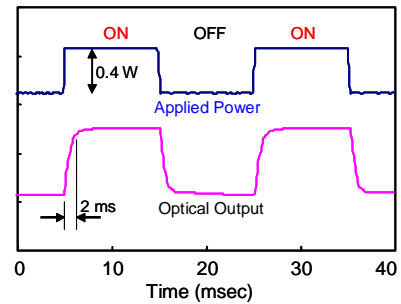


Fig.8 Time response of MZI

### 3.2 USE AS VARIABLE OPTICAL ATTENUATOR

A single MZI can be used as a variable optical attenuator if the electrical power to the heaters is controlled at a proper value ensuring a phase shift of less than  $\pi$ .

There are prospective attenuator applications where a response time of less than 1 ms is necessary to stabilize the output power of an optical amplifier without changing the pumping power and to equalize the output power between lasers without changing the injection current change. A high frequency pre-emphasis method has been proposed with which to improve the response time [8]. The heat diffusion delay from the heater to the waveguide core corresponds to a low pass filter response with a cut-off frequency of about 170 Hz. So it is possible to shorten the response time by driving the heaters with a simple electrical circuit that has a high frequency emphasized response. A response time of about 0.4 ms has been obtained experimentally with this method.

Although, in general, an MZI switch is polarization dependent as regards the thermo-optic effect due to compression stress from the substrate, there is no problem if the extinction ratio is over a specified value, for example 25 dB, for any polarization state. However, when used as an attenuator, the MZI transmittance should be constant at a given value, for example -10 dB, for any polarization state. The transmittance fluctuation results in the attenuator experiencing PDL. When we use the *through* path of the MZI, the PDL is about 0.25 dB at 10 dB attenuation since the polarization dependence of the thermo-optic effect is 3 % [9]. A heat-insulating groove is effective in reducing the PDL, as well as for reducing power consumption, because it also acts as a stress-releasing groove. With the groove, the polarization dependence is reduced to 0.6 % and the PDL is expected to be 0.05 dB at an attenuation of 10 dB.

### 3.3 128-WAY SELECTION SWITCH

Figure 9 shows a schematic and a photograph of a 128-way selection switch. A tree structure composed of a  $1 \times 2$  MZI element is used for 128-way output selection and each output is equipped with a gate switch to achieve a high extinction ratio when the output is not selected. A total of 255 MZI elements are integrated in a  $77 \times 40$  mm PLC chip by using a super high  $\Delta$  waveguide and the "driver IC on PLC" structure shown in Fig. 4(c) [5]. The average insertion loss over the 128 output paths is 2.6 dB and the average extinction ratio is 63 dB. The number of heaters to be activated depends on the output port and the average number is 4.5. The average power consumption is 1.6 W.

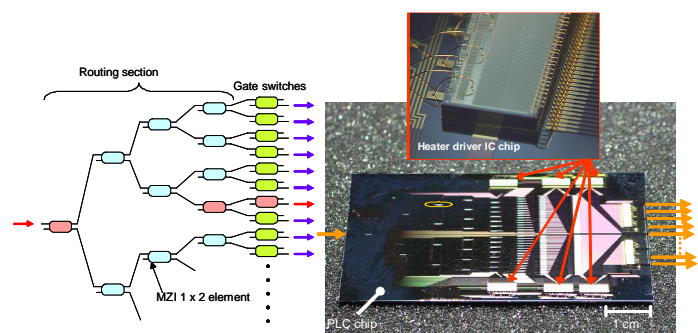


Fig.9 Schematic and chip photo of 1 x 128 switch

### 3.4 16 x 16 MATRIX SWITCH

The left side of Fig. 10 shows the logical connection diagram of an  $N \times N$  matrix switch ( $N=4$ ) composed of  $N^2$   $2 \times 2$  switch units. Each  $2 \times 2$  unit has a double gate structure as shown in the inset to double the extinction ratio. The photograph in Fig. 10 shows a packaged  $16 \times 16$  matrix module [4]. In this device, 512 MZI elements are integrated in a  $10 \times 10$  cm PLC chip and the waveguide length from input to output is 66 cm. The module has the "driver IC on PWB" structure shown in Fig. 4(b) and is  $165 \times 160 \times 23$  mm<sup>3</sup> in size. This switch can be operated by a signal from a PC or the control board of the transmission equipment. The average insertion loss over 256 (=  $16 \times 16$ ) paths is 5.6 dB and the average extinction ratio is 58.9 dB.

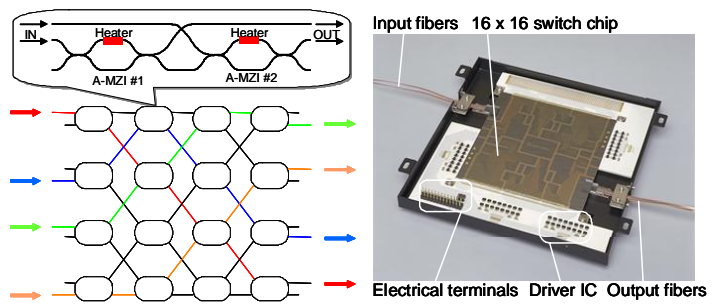


Fig.10 Schematic ( $N=4$ ) and module photo of  $16 \times 16$  switch

## 4. ASYMMETRIC MZI BASED DEVICES

### 4.1 SINGLE STAGE ASYMMETRIC MZI

An asymmetric MZI with a large path length difference as shown in Fig. 11 has a sinusoidal spectral response as a function of wavelength/frequency. Its period, or free spectral range (FSR), is given by

$$FSR = \frac{C}{n_g \cdot \Delta L} \text{ [Hz]} \quad \text{where } n_g = n_{c0} + f_0 \cdot \frac{dn_c}{df}$$

where  $C$  is the speed of light,  $\Delta L$  is the path length difference between the two waveguides and  $n_c$  is the effective refractive index of the propagation mode of the waveguides.  $f_0$  is the center optical frequency of the discussed frequency range and  $n_{c0}$  is  $n_c$  at  $f_0$ .  $n_g$  is called the group refractive index. The spectral responses of the two outputs are shifted by half a period as shown in the figure. The asymmetric MZI can be used as a frequency filter, a frequency locker for a laser diode, a demodulator for differential phase shift keying (DPSK) and an optical frequency counter. The advantage of fabricating the asymmetric MZI by using a PLC rather than fiber/bulk optics is that it enables us to obtain a highly accurate frequency response. Moreover, the MZI is compact and extremely stable. For example,  $\Delta L$  is about 2 cm for a DPSK demodulator of a 10 Gb/s transmission. The chip size is several centimeters and the chip can be packaged with a thermo-electric cooler. The temperature dependence of the frequency response is only  $-1.4$  GHz/ $^{\circ}\text{C}$  and we can stabilize it to within 1 GHz error by controlling the temperature with an accuracy of  $0.1$   $^{\circ}\text{C}$ . Its stability has been experimentally confirmed in a number of transmission experiments [10]. Polarization dependence caused by waveguide birefringence can be eliminated by inserting two half waveplates between the two couplers as described in Section 5.2.

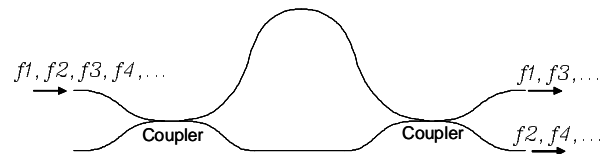


Fig.11 Asymmetric MZI

### 4.2 INTERLEAVE FILTER

The cascaded asymmetric MZI shown in Fig. 12 has a spectral response with a flatter and wider bandwidth than a single MZI [11]. This device is used to demultiplex dense DWDM light into two (odd and even) channel groups. With a combination of this device and two wavelength demultiplexers, it is possible to double the wavelength channel count of DWDM systems. To obtain a flat and wide transmission/rejection band, the coupling ratio of the coupler and the delay line length ( $\Delta L$  and  $2\Delta L$ ) should coincide accurately with their designed values. A stabilized coupler composed of a small path length difference MZI is used, whose coupling ratio is determined by  $\delta L$  and is stable against variations in the coupling ratio  $K$  of the individual couplers [12]. The delay time of the delay line can be adjusted by the permanent refractive index change method.

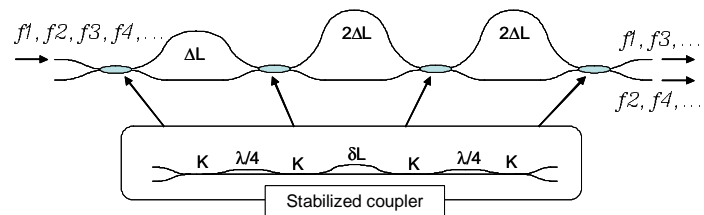


Fig.12 Waveguide layout of interleave filter

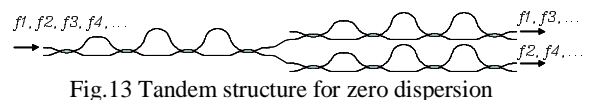


Fig.13 Tandem structure for zero dispersion

The upper and lower outputs in Fig. 12 have the same absolute chromatic dispersion values but one is positive and the other is negative. To eliminate the dispersion, one more circuit, which has the opposite dispersion value, is connected to each output port as shown in Fig. 13 [13]. Figure 14 shows transmission and chromatic dispersion spectra of a fabricated interleave filter, which demultiplexes DWDM light with a 50 GHz spacing into two components with a 100 GHz spacing. The packaged module has an average insertion loss of 1.9 dB, which includes waveguide-fiber coupling loss and connector loss. The dispersion is within  $\pm 20$  ps/nm. The PDL is reduced to less than 0.2 dB with a birefringence elimination technique.

### 4.3 DISPERSION COMPENSATORS

Optical pulse deformation due to dispersion is one of the problems that must be overcome if we are to realize high speed, long haul, and large capacity transmission. Dispersion compensation fibers can eliminate most chromatic dispersion in the transmission line but other adaptive compensators are needed to eliminate residual dispersion and dispersion variation in a large wavelength region over the WDM channels.

The cascaded asymmetric MZI shown in Fig. 15 works as a tunable dispersion compensator [14]. The variable coupler is a symmetric MZI with a thermo-optic phase shifter (as with the switch described above). By changing the coupling ratio of the variable coupler and phase shifters in the asymmetric MZI, we can obtain arbitrary dispersion dynamically. The path length difference  $\Delta L$  is designed so that the FSR matches the channel spacing of the DWDM light and simultaneous dispersion compensation for all WDM channels is possible. Figure 16 shows the measured group delay and transmittance in the vicinity of 1552.524 nm. We can change the dispersion value from -150 to 150 ps/nm and the insertion loss ranges from 4 to 4.6 dB. In this prototype, there are 7 variable couplers and 6 asymmetric MZIs, which include a total of 13 thermo-optic phase shifters. The electrical power applied to each heater (phase shifter) is measured in advance for each dispersion value and is preset in the control circuit in the packaged module. We can obtain an arbitrary dispersion value simply by sending a signal from a PC. The widest dispersion range is, in principle, proportional to the number of cascaded asymmetric MZIs and the maximum range obtained thus far is -681 to +786 ps/nm [15].

Figure 17 shows the operating principle of a multichannel dispersion compensator whose waveguide layout is the same as that of the interleave filter shown in Fig. 13 [16]. The first and second interleave filters have concave and convex group delay responses, respectively. If the centers of the concave and convex curves coincide, there is no group delay tilt (this is the reason for the tandem configuration of the zero dispersion interleave filter). However, the free spectral ranges of the first and second filters are intentionally different and the difference between the curve centers gradually increases. This causes

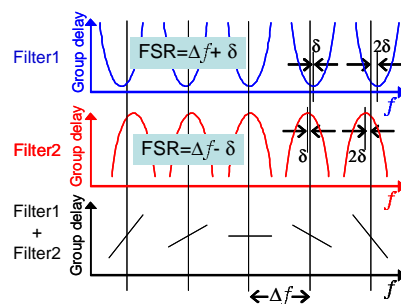


Fig.17 Principle of multichannel dispersion compensator

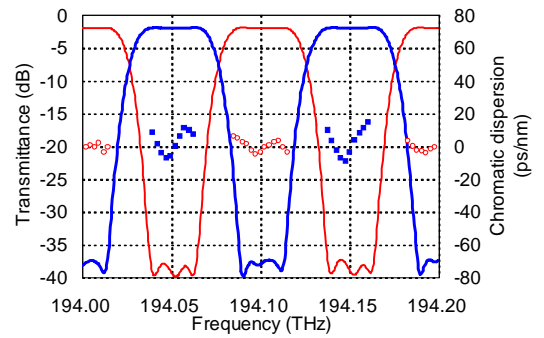


Fig.14 Spectrum of 50G/100G interleave filter

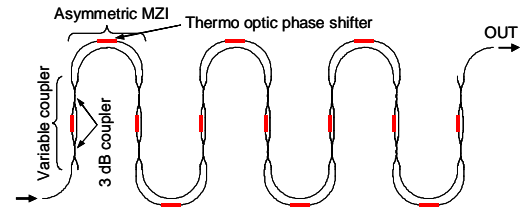


Fig.15 Cascaded MZI dispersion compensator

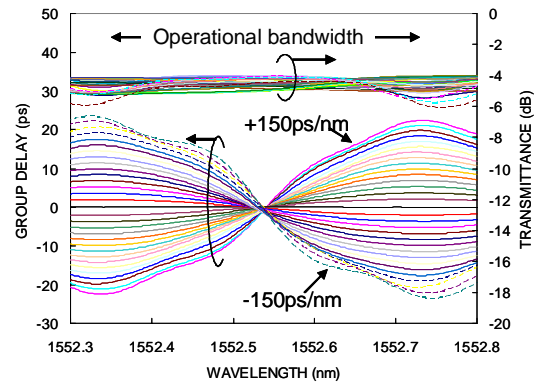


Fig.16 Characteristics of dispersion compensator in Fig.15

Figure 17 shows the operating principle of a multichannel dispersion compensator whose waveguide layout is the same as that of the interleave filter shown in Fig. 13 [16]. The first and second interleave filters have concave and convex group delay responses, respectively. If the centers of the concave and convex curves coincide, there is no group delay tilt (this is the reason for the tandem configuration of the zero dispersion interleave filter). However, the free spectral ranges of the first and second filters are intentionally different and the difference between the curve centers gradually increases. This causes

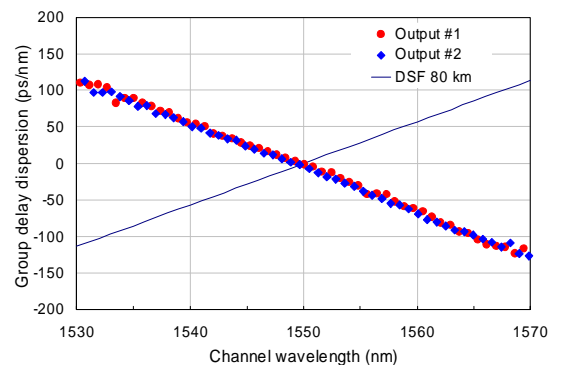


Fig.18 Dispersion of compensator and 80 km DSF

group delay tilt, i.e. dispersion, and the tilt changes with frequency channel. In the demonstration experiment, the FSRs were designed to be 100.4 and 99.6 GHz, respectively, and to have a dispersion slope of  $-5.7 \text{ ps/nm}^2$ , which corresponds to the reverse value for an 80 km long dispersion shifted fiber. Figure 18 is the measured dispersion at 100 channels with a spacing of 50 GHz. The circles and diamonds denote odd and even channels obtained at outputs #1 and #2, respectively. As designed, the obtained dispersion values are opposite to that for the DSF and so it is possible to cancel the dispersion slope of the transmission line with this device.

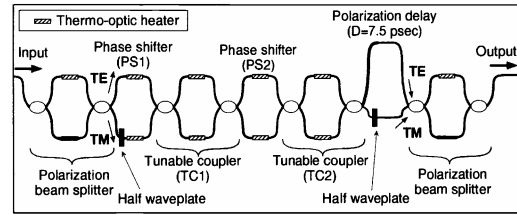


Fig.19 Circuit layout of PMD compensator

Polarization mode dispersion (PMD) is also a barrier to high bit rate transmission. Figure 19 shows the circuit layout of a PMD compensator using cascaded MZIs [17]. The input light is divided into TE and TM modes by the first MZI-based polarization beam splitter. It has two waveguides with different widths so that the MZI is symmetric for the TM mode and asymmetric for the TE mode. The TM mode is converted to the TE mode by a half waveplate. The two TE modes are phase-adjusted by a phase shifter (PS1) and combined with a proper coupling ratio by the first tunable coupler (TC1). Another phase shifter and tunable coupler (PS2 and TC2) combination is used together with a PS1 and TC1 for endless tracking operation. The intra-mode delay time difference of the input light is eliminated by the delay line. Finally, the light is recombined by the second polarization beam splitter and transmitted toward the output. Figure 20 shows the measured power penalty at a bit error rate of  $10^{-9}$  with and without the PMD compensator. It is found that the compensator extends the allowable PMD from 5.5 to 12 ps for a 1 dB penalty.

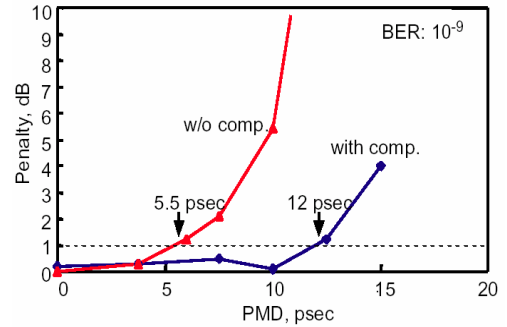


Fig.20 Power penalty reduction with PMD compensator in Fig.19

#### 4.4 GAIN SPECTRUM EQUALIZERS

It is necessary to flatten the gain spectrum of an optical fiber amplifier to equalize the optical power across all the WDM channels, especially in a long haul system where many amplifiers are cascaded. A simple solution is to use variable attenuators for individual channels between a wavelength demultiplexer and a multiplexer. However, the spectral response is discrete and can only be used in a fixed-wavelength channel system. Here, two PLC based gain spectrum equalizers with a non-discrete spectral response are described.

Figure 21 is a Fourier series type gain equalizer composed of asymmetric MZIs with different FSRs [18]. The arbitrary loss spectrum needed for equalization is synthesized from a series of sinusoidal responses with different periods. Each asymmetric MZI contains two symmetric MZIs as variable couplers instead of simple 3 dB directional couplers. This structure enables us to obtain sinusoidal curves with arbitrary amplitudes. The thermo-optic phase shifters are used to shift the phase of the sinusoidal curves. If there are more MZIs, the fidelity of the synthesized spectrum increases. The difference between the synthesized and target spectral curves results in a residual ripple in the equalized spectrum. Figure 22 shows an experimental result where the ASE spectrum from an  $\text{Er}^{3+}$ -doped tellurite fiber amplifier was flattened. Here the fabricated equalizer has 10 MZIs and excellent equalization is obtained with a residual ripple of 0.9 dB over a 69 nm range. The insertion loss is 9 dB, which includes an SMF-SHA waveguide coupling loss of 3 dB, and 3 dB excess losses in the polarization beam splitter and circulator used for the polarization diversity technique. If these experimental losses are improved, the insertion loss will be 3 dB.

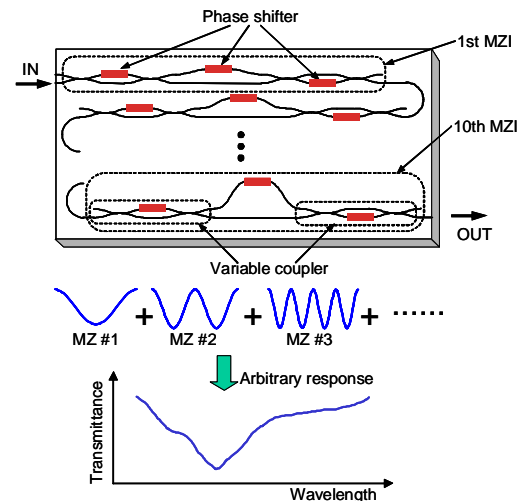


Fig.21 Principle of Fourier-series gain equalizer

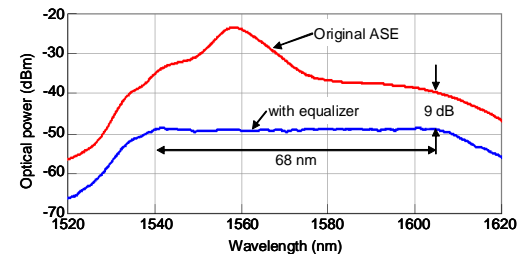


Fig.22 Original and equalized ASE spectrum

Another way to equalize the gain spectrum is to use a transversal filter structure in which the input is split into N components with different

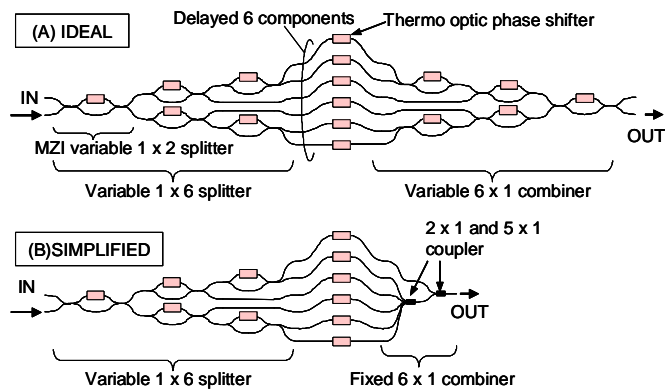


Fig.23 Transversal type gain spectrum equalizer

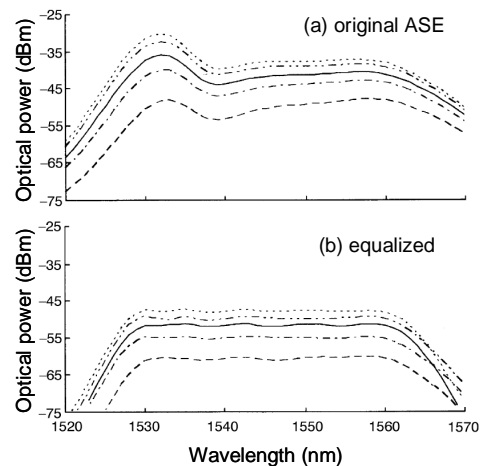


Fig.24 Equalization experiment results

amplitudes and phases and combined to the output [19]. It is mathematically proven that an arbitrary spectral response can be realized by using this structure. Figure 23(a) is an ideal circuit pattern of  $N=6$ . The variable  $1 \times 6$  splitter used to obtain different amplitudes is composed of symmetric MZIs. The phase shifter array is used for controlling the phase of the 6 components. There is no excess loss in the combiner because the whole circuit layout is mirror-symmetric. To reduce the circuit length and total electrical power consumption of the heaters, a simplified layout (b) where the coupling ratio of the combiner is fixed is useful if the target is limited to a certain spectrum, for example, that of an EDFA. Figure 24 shows experimental results for equalization with the simplified circuit. The same experiments were repeated changing the original spectral pattern of EDFA with different pumping powers. All the different ASE spectra from an EDFA were successfully equalized. This demonstrates the feasibility and adaptability of the transversal-type equalizer.

## 5. ARRAYED-WAVEGUIDE GRATING WAVELENGTH MULTIPLEXER

### 5.1 PRINCIPLE AND BASIC CHARACTERISTICS

An arrayed-waveguide grating (AWG) is composed of hundreds of channel waveguides with different lengths and acts as a transmissive diffraction grating [20,21]. An AWG is usually integrated with input and output waveguides and two slab waveguides as shown in Fig. 25. Input light diffracts in the input slab and excites the hundreds of waveguides in the AWG in phase. All the waveguide axes are aimed at the center of the output slab waveguide edge and the radiation from the AWG converges at the center as shown in Fig. 26(a) when the length difference between the waveguides in the AWG is an exact multiple of the input wavelength (this wavelength is called the center wavelength). When the input wavelength is shifted from the center wavelength, the optical phase at the waveguide exits of the AWG is tilted as shown in Fig. 26(b). As a result, the point of convergence is shifted to the other output waveguide entrance and the WDM input light is demultiplexed to different output waveguides.

The transmission spectrum in the vicinity of the center wavelength is normally Gaussian because the mode field pattern at the junction of the input waveguide and the input slab determines the spectrum and it is approximately Gaussian. It is possible to obtain other spectra by changing the mode field. With a wide input waveguide aperture at the junction, the spectrum is wide Gaussian. With a parabolic input waveguide, it becomes a flat-top curve [22]. Figure 27 shows three typical spectra. All devices were designed to have a channel spacing of 0.8 nm. The 3 dB bandwidths for Gaussian, flat-top and wide Gaussian devices are 0.4, 0.6 and 0.7 nm, respectively. The transmittance, bandwidth and adjacent channel suppression have a trade-off relationship, and one of the three types and an intermediate design are chosen according to the desired application. Typical transmission spectra for all channels are shown in Fig. 28. This sample has 48 channels with a 100 GHz spacing and a Gaussian response,

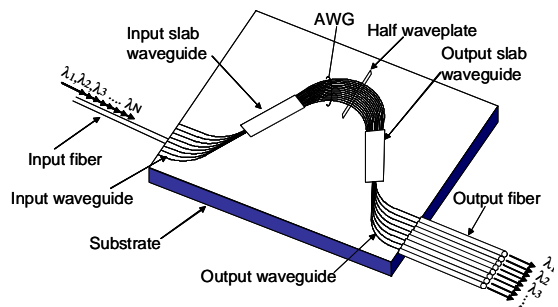


Fig.25 Schematic of AWG wavelength multiplexer

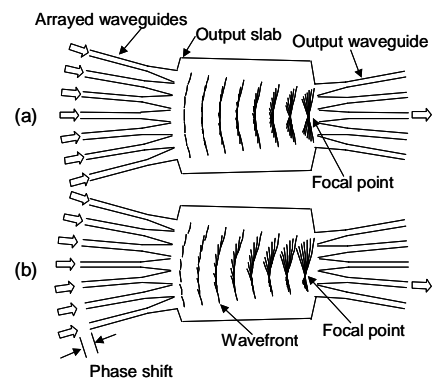


Fig.26 Interference in output slab; a) center wavelength b) shifted wavelength

and the insertion loss variation is very small (< 1 dB). All 48 channels have the same spectrum, which simplifies the WDM system design.

## 5.2 DISPERSION AND POLARIZATION SENSITIVITY

In principle, the group delay dispersion of an AWG wavelength multiplexer is zero, unlike other interference-based filters such as dielectric multilayer filters and fiber Bragg gratings. Although there is some dispersion due to phase error at the waveguide exits of an AWG caused by inhomogeneity as regards the thickness and refractive index of the core layer [23], the experimental value is as small as  $\pm 5$  ps/nm for a 0.8 nm spacing, Gaussian AWG. In general, as the channel spacing becomes narrower, the dispersion becomes larger. The phase error of the individual waveguides in an AWG can be analyzed by using low coherence Michelson interferometer based measurement systems [24] and it can be adjusted to zero using the UV light irradiation method [25]. This technique will be useful for realizing a low dispersion AWG with a very narrow channel spacing of 0.2 nm (25 GHz) or less.

Generally, waveguides have polarization dependence with respect to propagation loss and refractive index. Our silica-based waveguide has a square cross-section and its loss is isotropic. However it has birefringence due to thermal stress, and the TE and TM mode spectra are slightly shifted by about 0.1 nm. To overcome this, the polarization mode conversion technique is more useful than birefringence reduction techniques that employ stress control, which usually depend on fabrication process conditions. For mode conversion, we use a half waveplate inserted in a groove that traverses the middle of the AWG as shown in Fig. 25 [26]. Its principal optical axis is at 45 degrees to the waveguide surface and the waveplate rotates the TE mode to the TM mode and vice versa. So the refractive indices of the TE and TM incident lights have the same value (average of TE and TM) and the polarization dependence is completely eliminated whatever the birefringence. This technique is unaffected by the fabrication process and the yield is very high. The insertion loss caused by the groove is less than 0.5 dB [27]. The polarization mode dispersion (PMD) of the AWG multiplexer is negligible (approximately equal to the measurement error of 0.1 psec) because the device length is several centimeters at most in addition to use of the half waveplate.

## 5.3 CHALLENGES FOR HIGH CHANNEL COUNT AND LOW LOSS

At present, the channel count and channel spacing of commercial AWG wavelength multiplexers used in dense WDM systems are 8 to 64 and 200 GHz (1.6 nm) to 50 GHz (0.4 nm), respectively. Although there is no need for higher performance (narrower spacing and higher channel count) because of the current recession in the IT industry, research and development are proceeding for prospective applications not only in optical fiber communication but also in such areas as signal processing. The channel spacing  $\Delta\lambda$  of the multiplexer is given by

$$\Delta\lambda = \frac{n_s \cdot d}{f \cdot m} \cdot \frac{n_c}{n_g} \cdot \Delta x$$

where  $n_s$  and  $n_c$  are the effective refractive indices of a slab waveguide and a channel waveguide, respectively and  $n_g$  is the group index of a channel waveguide.  $\Delta x$  and  $d$ , indicate the spacing of the output and arrayed waveguides, respectively.  $f$  and  $m$  are the focal length of the slab waveguides and the diffraction order, respectively. This equation shows that focal length  $f$  should be longer for a narrower channel spacing, which is necessary for a higher channel count. The number of waveguides in an AWG should be large in order to receive the whole diffracted light power in the slab waveguide without loss. So a high channel count AWG requires good homogeneity in terms of refractive index and glass layer thickness throughout a large circuit area. The highest channel count yet obtained is 512 with a channel spacing of 10 GHz (0.08 nm) [28]. The whole circuit including two slab waveguides with a focal length of 74 mm and 1337 waveguides in AWG was contained on a 4 inch substrate by using 1.5%- $\Delta$  waveguide.

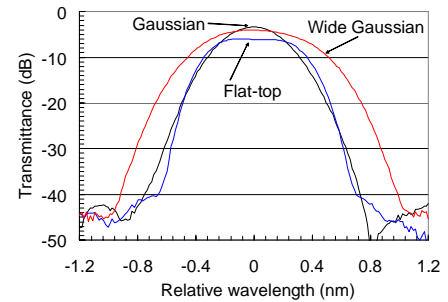


Fig.27 Typical AWG spectra

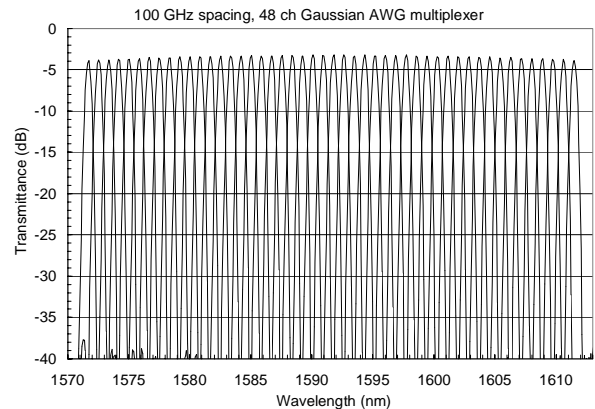


Fig.28 Transmission spectra of 48 channel AWG

When the PLC chip is composed of a 1.5%- $\Delta$  waveguide, the waveguide-fiber coupling loss is high. The spot size conversion method is effective in reducing this and was successfully demonstrated through the realization of the 25 GHz spacing, 256 channel AWG multiplexer module shown in Fig. 29 [29]. The AWG chip and the fan-out waveguide array chip are composed of 1.5%- $\Delta$  and 0.75%- $\Delta$  waveguides, respectively and taper structures are introduced at the chip-to-chip junction and chip-to-fiber junction as shown in Fig. 2. A thermally expanded core (TEC) junction is used between the input SMF (not shown in the figure) and a high-NA fiber. As a result, a low insertion loss of 1.9 dB is obtained for central channels and 3.9 dB for outer channels.

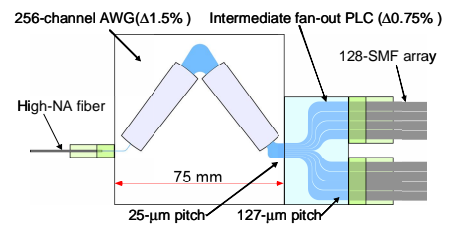


Fig.29 Configuration of 256 ch AWG

The insertion loss of the AWG multiplexer module mainly consists of waveguide propagation loss, waveguide-fiber coupling loss and mode conversion loss at the AWG/slab junction. By using the silica PLC technology described above, the first two factors become negligible and the last becomes the object of our attention. As shown in Fig. 26, the ends of the channel waveguides are widened with a taper structure at the slab junction. Gaps remain between the waveguide ends due to the resolution limits of photolithography and dry etching. This results in a conversion loss from the in-slab plane wave to the channel waveguide propagation mode. This loss can be reduced by introducing a sloped structure between the arrayed waveguide cores as shown in Fig. 30, which provides light with a smooth adiabatic transition [30]. The slope structure can be made with a special condition when dry-etching the core that is based on the fact that the etching rate is lower where gap between the cores is narrower. The loss reduction provided by this method is 1 dB or more and its repeatability is experimentally confirmed.

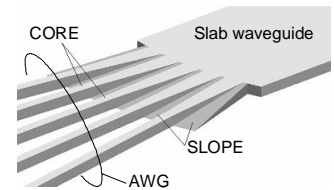


Fig.30 Slope for loss reduction

## 6. FUTURE OF PLC TECHNOLOGY

### 6.1 ROAD MAP

Figure 31 summarizes the developments we have made using silica-based PLCs in addition to the devices and techniques described above. Although this map is based on device development history, not all the devices have been put to practical use since their application system development is still under way and awaits increased traffic demand. Some devices will be needed and brought to completion at that time. In this sense, the figure offers a road map for PLC technology from now to the near future.

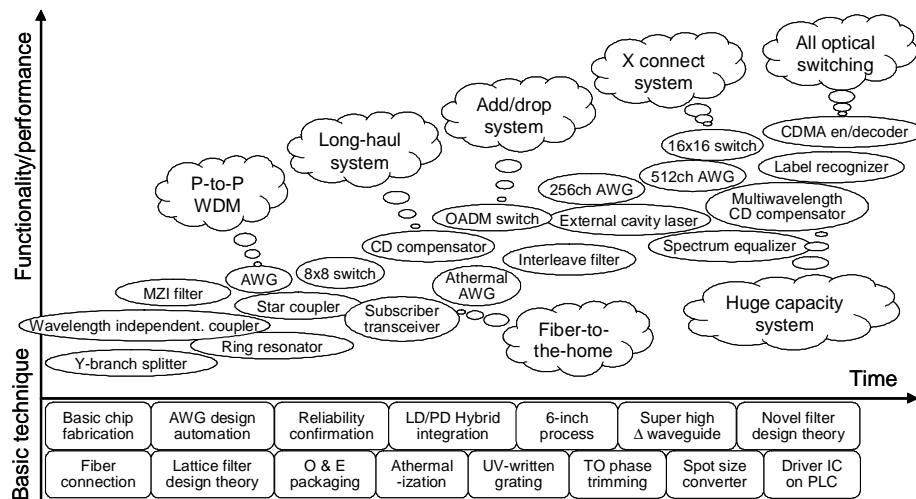


Fig.31 Fundamental technology, devices and prospective application systems of PLC

### 6.2 NEXT R & D TARGETS

**1) Large scale circuit for higher performance:** Even if the functionality remains the same, the circuit scale of devices will probably have to increase as transmission systems expand. Examples include the channel count of the AWG wavelength multiplexer and the port count of the switch. One way to realize this is to increase circuit density by using a waveguide with a  $\Delta$  higher than 1.5 %. This would make it possible to reduce the waveguide bending radius to less than

2 mm. It is easy to increase the concentration of Ge in a silica core to realize a higher  $\Delta$  but this approach increases the propagation and fiber connection losses. We must improve the etching process and spot size conversion technique to combat these two types of degradation. The other way is to increase the chip size by using Si wafers of 8 inches or more. Since the same or better homogeneity than the present process is required for a wide circuit area, the fabrication process must be improved to provide good control of the thickness and refractive index of the silica layer.

**2) Integration for size and cost reduction:** Clearly, the on-chip integration of optical elements with different functions will lead to size reduction, the elimination of fiber connection and finally to cost reduction. An optical add/drop circuit is a typical example, which includes a pair of AWGs for multi/demultiplexing and a  $2 \times 2$  switch array [31]. This device can add and drop arbitrary wavelength channels of WDM light. The integration of a variable attenuator array with a wavelength multiplexer is also useful for realizing a one-board WDM transmitter with large wavelength channels. The optimum conditions in the fabrication processes for different elements, for example, the AWG and thermo-optic switch, are slightly different at present. We must improve the fabrication process to find conditions that are suitable for both elements. Non-silica elements such as laser diodes, photo diodes and lithium niobate modulators can also be integrated with silica based PLCs. This hybrid integration makes it possible to realize one-chip WDM transmitters and receivers [32,33]. The basic principles of this technology have been established and individual developments for practical applications are in progress.

**3) New circuits for new systems:** Although devices based on silica PLCs are passive, their applications are infinite. AWG wavelength multiplexers and thermo-optic switches are just the tip of the iceberg. It is mathematically proven that lattice form filters (cascaded MZI structure) and transversal filters can realize arbitrary frequency responses. At present, they are used only for dispersion compensators and spectrum equalizers. In addition, a combination circuit composed of delay lines is simple to fabricate but has high functionality in certain circumstances. A label recognition circuit is a clear example [34]. A high-speed pulse train (optical label) input is divided into delay lines and recombined with a different delay time and amplitude. When the label coincides with the set delay pattern, an output pulse is launched. Another combination of variable delay lines and an AWG is also experimentally shown to function as the encoder/decoder of a time-spreading/wavelength-hopping optical CDMA circuit [35]. Additionally, revivals of simple circuits such as an MZI and a ring resonator should not be overlooked. They can be used as an optical DPSK decoder and a chromatic dispersion compensator, respectively. The original ideas were proposed many years ago but there was no way of realizing them at that time because the stability and accuracy of bulk optics were insufficient. Now we have PLC technology and the exploration for new applications has just begun.

## 7. CONCLUSION

This paper outlined recent trends related to silica-based PLCs and introduced principles and experimental results in connection with devices fabricated in NTT laboratories. These devices have excellent characteristics and it is confirmed that there are no problems related to the chip fabrication process, fiber attachment, packaging or reliability. Some devices have already been introduced in practical transmission systems. So it can be said that basic PLC technology is now established. The next targets for research and development are the creation of new optical circuits with novel functions and the integration of different optical elements to achieve high performance, respectively.

## REFERENCES

1. A. Himeno et al., "Silica-based planar lightwave circuits", IEEE J. Selected Topics in Quantum Electronics, vol. 4, no. 6, pp. 913-924, 1998
2. M. Kawachi, "Silica waveguides on silicon and their application to integrated-optic components", Optical and Quantum Electronics, vol. 22, pp. 391-416, 1990
3. M. Ishii et al., "Low-loss fibre-pigtailed 256 channel arrayed-waveguide grating multiplexer using cascaded laterally-tapered waveguides", Electronics Letters, vol. 37, no. 23, pp. 1401-1402, 2001
4. T. Shibata et al., "Silica-based  $16 \times 16$  optical matrix switch module with integrated driving circuits", Optical Fiber Communication Conference, vol. 3, pp. WR1-1, 2001
5. S. Mino et al., "Novel IC-on-PLC technology and its application to compact  $1 \times 128$  silica-based PLC switch", Optical Fiber Communication Conference, TuE2, 2003
6. Y. Hibino et al., "High reliability optical splitters composed of silica-based planar lightwave circuits", Journal of Lightwave Technology, vol. 13, No. 8, pp. 1728-1735, August 1995
7. T. Goh, "Recent advances in large-scale silica-based thermo-optic switches", Proceedings of SPIE, Asia-Pacific optical and wireless communications, vol. 4582, pp. 49-56, 2001
8. T. Kawai et al., "PLC type compact variable optical attenuator for photonic transport network", Electronics Letters, vol. 34, no. 3, pp. 264-265, 1998
9. Y. Inoue et al., "Polarization sensitivity of a silica waveguide thermo-optic phase shifter for planar lightwave circuits", Photonics Technology Letters, vol. 4, no. 1, pp. 36-38, 1992

10. Y. Miyamoto et al., "S-band WDM coherent transmission of 40 x 43-Gbit/s CS-RZ DPSK signals over 400 km DSF using hybrid GS-TDFAs/Raman amplifiers", *Electronics Letters*, vol. 38, no. 24, pp. 1569 -1570, 2002
11. M. Oguma et al., "Flat-passband interleave filter with 200 GHz channel spacing based on planar lightwave circuit-type lattice structure", *Electronics Letters*, vol. 36, no. 15, pp. 1299 -1300, 2000
12. M. Oguma et al., "Compactly folded waveguide-type interleave filter with stabilized couplers", *Optical Fiber Communication Conference, TuK3*, 2002
13. T. Chiba et al., "Chromatic dispersion free Fourier transform-based wavelength splitter for DWDM", *Opto-Electronics and Communications Conference, Technical digest*, pp. 374-375, 2000
14. S. Suzuki et al., "Low-loss integrated-optic dynamic chromatic dispersion compensators using lattice-form planar lightwave circuits", *Optical Fiber Communication Conference, TuE7*, 2003
15. K. Takiguchi et al., "Variable group-delay dispersion equalizer using lattice-form programmable optical filter on planar lightwave circuit", *Journal of Selected Topics in Quantum Electronics*, vol. 2, no. 2, pp. 270-276 1996
16. M. Oguma et al., "Multi-channel chromatic dispersion compensator consisting of modified interleave filter", *Optical Fiber Communication Conference, FJ7*, 2003
17. T. Saida et al., "Planar lightwave circuit polarization-mode dispersion compensator", *Photonics Technology Letters*, vol. 14, no. 4, pp. 507-509, 2002
18. K. Suzuki et al., "PLC-based dynamic gain equalizer consisting of integrated Mach-Zehnder interferometers with C- and L band equalising range", *Electronics Letters*, vol. 38, no. 18, pp. 1030 -1031, 2002
19. T. Saida et al., "Dynamic gain equalisation filter based on integrated optical transversal filter with asymmetric combiner", *Electronics Letters*, vol. 38, no. 12, pp. 560 -561, 2002
20. M. K. Smit, "New focusing and dispersive planar component based on an optical phased array", *Electronics Letters*, vol. 24, no. 7, pp.385-386, 1988
21. H. Takahashi et al., "Wavelength multiplexer based on SiO<sub>2</sub>-Ta<sub>2</sub>O<sub>5</sub> arrayed-waveguide grating", *Journal of Lightwave Technology*, vol. 12, no. 6, pp. 989-995, 1994
22. K. Okamoto, "Flat spectral response arrayed-waveguide grating multiplexer with parabolic waveguide horns", *Electronics Letters*, vol. 32, pp. 1661-1662, 1996
23. H. Yamada et al., "Dispersion resulting from phase and amplitude errors in arrayed-waveguide grating multiplexers-demultiplexers", *Optics Letters*, vol. 25, no. 8, pp.569-571, 2000
24. K. Takada et al., "Optical low coherence method for characterizing silica-based arrayed-waveguide grating multiplexers", *Journal of Lightwave Technology*, vol. 14, pp. 1677-1689, July 1996.
25. K. Takada et al., "Beam-adjustment-free crosstalk reduction in a 10 GHz-spaced arrayed-waveguide grating via photosensitivity under UV laser irradiation through a metal mask, " *Electronics Letters*, vol. 36, pp. 60-61, 2000.
26. H. Takahashi et al., "Polarization-insensitive arrayed-waveguide grating wavelength multiplexer on silicon", *Optics Letters*, vol. 17, pp. 499-501,1992
27. Y. Inoue et al., "Polarization mode converter with polyimide half waveplate in silica-based planar lightwave circuits", *Photonics Technology Letters*, vol. 6, no. 5, pp. 626-628, 1994
28. K. Takada et al., "Low-crosstalk 10-GHz-spaced 512-channel arrayed-waveguide grating multi/demultiplexer fabricated on a 4-in wafer", *Photonics Technology Letters*, vol. 13, no. 11, pp. 1182-1184, 2001
29. M. Ishii et al., "Low-loss fibre-pigtailed 256 channel arrayed-waveguide grating multiplexer using cascaded laterally-tapered waveguides", *Electronics Letters*, vol. 37, no. 23, pp. 1401-1402, 2001
30. A. Sugita et al., "Very low insertion loss arrayed-waveguide grating with vertically tapered waveguides", *Photonics Technology Letters*, vol. 12, no. 9, pp. 1180 -1182, 2000
31. T. Saida et al, "Athermal silica-based optical add/drop multiplexer consisting of arrayed waveguide gratings and double gate thermo-optic switches", *Electronics Letters*, vol. 36, No. 6, pp. 528-529, 2000
32. T. Tanaka et al., "Hybrid-integrated external-cavity laser without temperature-dependent mode hopping", *Journal of Lightwave Technology*, vol. 20, no. 9, pp. 1730-1739, 2002
33. S. Mino, "Advances in PLC hybrid integration technology", *Integrated Photonics Research, Technical digest*, pp. 88-90, 2003
34. T. Saida et al., "Integrated optical digital-to-analogue converter and its application to pulse pattern recognition". *Electronics Letters*, vol. 37, no. 20, pp. 1237-1238, 2001
35. K. Takiguchi et al., "Encoder/decoder on planar lightwave circuit for time-spreading/wavelength-hopping optical CDMA", *Electronics Letters*, vol. 38, no. 10, p. 469, 2002